

Multimode Fiber Projector

Babak Rahmani,^{1,*} Damien Loterie,¹ Eirini Kakkava,² Navid Borhani,² Uğur Teğın,^{1,2} Demetri Psaltis,² Christophe Moser,¹

¹*Ecole Polytechnique Fédérale de Lausanne, Laboratory of Applied Photonics Devices, CH-1015 Lausanne, Switzerland*

²*Ecole Polytechnique Fédérale de Lausanne, Laboratory of Optics, CH-1015 Lausanne, Switzerland*

*Corresponding author: babak.rahmani@epfl.ch

Direct image transmission in multimode fibers (MMFs) is hampered by modal scrambling inside the fiber due to the multimodal nature of the medium. To undo modal scrambling, approaches that either use interferometry to construct a transmission matrix or iterative feedback based wavefront shaping to form an output spot on the camera have been proposed and implemented successfully. The former method entails measuring the complex output field (phase and amplitude) using interferometric systems. The latter, requires scanning the spot by phase conjugation or iterative techniques to form arbitrary shapes, increasing the computational cost. In this work, we show that by using neural networks, we are able to project arbitrary shapes through the MMF without measuring the output phase. Specifically, we demonstrate that our *projector* network is able to produce input patterns that, when sent through the fiber, form arbitrary shapes on the camera with fidelities (correlation) as high as ~90%. We believe this approach opens up new paths towards imaging and pattern projection for a plethora of applications ranging from tissue imaging, surgical ablations to virtual/augmented reality.

1. Introduction

Recent years have witnessed a surge towards using MMFs for exploiting their large space-bandwidth product for communication and imaging. This has been made possible thanks to the availability of thousands of modes in MMFs. At the same time, this very advantage of MMFs is its own enemy. The energy splitting and transfer among different modes inside the fiber give rise to a distorted field at the output of the fiber, often referred to as speckle pattern. Several approaches have been proposed to compensate the modal dispersion in MMFs. Analog phase conjugation via holographic materials initially suggested by Wertz and Spitz in 1966¹ and later on via a third order nonlinear crystal by Yariv and co-workers²⁻⁴ was the first method proposed for recovering the distorted fields. Many decades later, digital holography and phase conjugation was carried out digitally on the computer⁵⁻⁹. Nevertheless, today it still requires an extremely accurate calibration and is significantly prone to perturbation. Alternatively, digital iterative algorithms implemented with spatial light modulators (SLMs) are used to shape the beam entering the MMF to form a focused spot at the output of the fiber¹⁰⁻¹⁴. By scanning the focused spot in the field of view of the fiber, an image can be produced.

Other methods use interferometry to measure the complex field at the output of the fiber and then construct a transmission matrix between the light modulator component (SLM for example) and the object on both sides of the MMF¹⁵⁻¹⁹. This method entails measuring the phase with holography. Additionally, after any small perturbation in the system the matrix should be re-measured which could be a challenging task in terms of time and computational resources.

It should be noted that out of the two major approaches for image transmission through the MMF, i.e. the digital iterative method and the transmission matrix, the former is limited to projecting simple and basic shapes such as focused spots but the latter can project any arbitrary pattern at the output of the fiber however it requires nontrivial experimental setup. The transmission matrix method is built based on the fact that the input-output optical field relationship in multimode fibers (and other scattering media) is linear and deterministic as long as no optical nonlinear process is initiated inside the fiber. A number of input patterns (basis vectors) modulated with either phase-, amplitude- or both are sent through the fiber and their corresponding complex output fields are measured. The matrix is simply the *linear* relationship between the input and output fields. It is interesting to ask the question: *if given several input-output examples from the MMF with the output examples being measured amplitude-only (no complex measurement), is it possible to project arbitrary shapes through the fiber?* Here, we seek an approach that has the simplicity of the optical setup used with the digital iterative methods and the generality in the range of shapes that the transmission matrix is able to project. In other words, we investigate the possibility of projecting arbitrary shapes at the output of a MMF by only using a SLM at the input and a camera at the output. Thus, our optical setup for image projection requires a simple apparatus, i.e. a spatial light modulator, a scattering medium and a camera. The schematic of such a system is depicted in Fig. 1. We start by first acquiring a number of inputs (SLM patterns) and outputs (camera intensity images) examples. Then, we try to establish a relationship between the two sets. This involves solving an *inverse nonlinear problem* from the *amplitude-only images captured by the camera* (phase information is lost as the intensity-only detection by camera is limited to acquiring the modulus of the electric field at the output of the fiber $|E(x, y)|^2$ and then taking the square root of the intensity images to obtain amplitude images; hence the expression *amplitude-only images captured by the camera*).

Neural networks are known to perform well in solving inverse problems²⁰⁻²¹. They are now being extensively used in many disciplines such as biology, computer vision, material sciences with applications ranging from super resolution microscopy of histology samples²² to inverse design of photonic devices²³ and materials²⁴.

Recently, neural networks were used to reconstruct the undistorted input fields of MMFs²⁵⁻²⁷ (and other types of scattering media²⁸⁻²⁹) from the amplitude-only scrambled speckle patterns at its output for fibers with various lengths that could reach as long as 1 kilometer²⁶. These works in particular show that neural networks can learn to reconstruct the input of the MMF from its output.

Here we intend to accomplish the reverse: to learn the correct inputs that will generate a desired output of the MMF. This is not trivial because we restrict ourselves to only send forward information (input to output). This is challenging because first and foremost, no straightforward way (without using the transmission matrix) exists for acquiring a training set with the desired output patterns to train the neural network. The training set for this task consists of examples of the desired shapes (for example recognizable drawings such as smiley face, alphabet letters, etc.) on the distal end of the fiber (camera side) and examples of the SLM patterns that generate those patterns when sent through the fiber. Unfortunately, this is exactly the problem we intend to solve. If we had those examples at hand, the problem would already be solved, making it a chicken and egg dilemma. Recently, an initial attempt towards projecting patterns through MMFs using neural networks has been made that is limited to focusing spots³⁰ after the fiber.

In this work, we use a combination of sub-neural networks (referred to as *the projector network* on the whole) to generate the SLM patterns that create the desired shapes on the camera. Specifically, our projector network, schematically depicted in Fig. 2a, is made of two sub-networks, the *Generator* and the *Discriminator*. The discriminator sub-network tries to learn the forward propagation path of the MMF (input to output) and the generator learns the inverse path. In other words, the generator network generates SLM patterns constrained by the physical propagation rules of the system which are embedded in the discriminator network D. The two networks are trained synergistically so that the discriminator forces the generator to generate SLM patterns that, upon sending through the fiber, produce images on the camera similar to the desired set. Training D to emulate the forward path of the light propagation in fact allows *in situ* back propagation of the error between the desired target images and what appears on the camera in the real experiment through the virtual fiber (i.e. D). When the back propagated error reaches G, the learnable parameters of the sub-network G is adjusted so as to the error is reduced. The error is the smallest when G is the inverse of D. Therefore, this training method, which has also been proposed for use in control systems (plants) nearly three decades ago³¹, is effectively trying to find the inverse path of light propagation or analogously the time reversal operator.

Specifically, the training of the two networks, depicted schematically in Fig. 2b, is carried out in the following way: initially neither of the networks is trained; hence we start collecting examples for training D. These examples consist of SLM images and their corresponding experimentally generated output speckle patterns on the camera. It should be noted that our goal here is to find a subset domain of SLM images that produce a certain class of images on the output of the fiber. In the beginning, we have no information about such a domain. Hence, in the first iteration, we choose random SLM images to send through the fiber and measure the amplitude-only images on the camera. We then, train the neural network D with this dataset. Once training of D is complete, we start training the second neural network G by feeding it with the class of images that we wish to project through the fiber. The weights of the network D

are kept fixed. G learns the mapping from the output amplitude images on the camera to the proper SLM images constrained with the physical propagation rules of the MMF which is modeled by D. By the end of the first iteration, the domain of the output SLM patterns generated by network G must have moved closer in some metrics (Euclidean distance, for example) to the domain of SLM images that produce the desired images at the output of the fiber. In the second iteration, the SLM images that were produced by the sub-network G in the previous iteration are loaded experimentally on the physical SLM and a new set of output images are captured by the camera. The network D is then trained with this new dataset. Once completed, the training of G is carried out in the same way as in the first iteration. Depending on the quality of images that are projected through the fiber, this process could be repeated a few times. It is expected that after each iteration, the domain of the SLM patterns generated by G gets closer to the domain of SLM images that produce the desired target images at the output of the fiber.

The architecture of the projector network is *reminiscent* of that of the so-called Generative Adversarial Networks (GANs). The similarity is rooted from the fact that the training of G, i.e. mapping from amplitude patterns to SLM images, cannot be straightforwardly carried out because no label (ground truth SLM images) for target output images exists *a-priori* (training cannot be performed in a supervised manner in which ground truth labels are available beforehand). Therefore, the performance of G gets better by working synergistically with D to generate SLM images that result in output amplitude images with higher fidelities. The training procedure is explained more formally in the Materials and Methods section.

We use our network to project images belonging to various dataset ranging from Latin alphabet, digits, as well as other drawings. We obtained fidelities (correlations) as high as 85% even when the projected image belongs to a category different from the one the neural network is trained with. This accounts for the ability of the network to generalize to class of images it has never seen which is critical for a general-purpose imaging system.

2. Results

The network (*projector + generator*) is trained on experimentally generated SLM-images and their corresponding amplitude images captured by a physical camera. See data preparation subsection in Materials and Methods for a detailed explanation. We use a dataset containing 20,000 images from EMNIST³¹ which contains grayscale images of handwritten Latin alphabet characters. Once the network is trained, we test its performance on 1000 unseen images of Latin alphabet as well as other class of images including 1000 MNIST digits, and random sketches. The image projection average fidelities for different dataset are reported in Table I.

Figure 3 depicts examples of the target images belonging to the training and testing sets and the physical outputs on the camera. The insets of the figures indicate the correlation of the two images.

Examples of the projected images on the camera obtained from the handwritten digits dataset are depicted in Fig. 4. For this, the network is trained only on one class of images (Latin alphabet) and is then directly tested on these other classes. This demonstrates the generalization ability of the neural network and the fact that it can extend its understanding to images never seen by the network even in the training step.

The generalization ability of the neural network is further demonstrated in Fig. 5 which shows examples of different random drawings projected through the fiber by using the SLM patterns produced by the network trained only on Latin alphabet. An example of these SLM patterns is plotted in Fig. 5. The corresponding targeted and projected images of this SLM pattern are shown as well. An animation of this target “Running Man” is provided in Supplementary Materials 1.

We additionally repeated the same experiment but used an extremely small dataset of 1000 handwritten Latin alphabet for training the network. The image projection average fidelities for different dataset are reported in Table I for the comparison with the previous experiment. The results show that for substantially smaller data size, projection fidelities are only slightly worse. On the other hand, looking into the fidelity trajectory of the projected images (see Materials and Methods and Supplementary Materials X) reveals that the neural network finds the required input SLM modulations of the target images quite rapidly (only after three rounds of training iterations).

3. Discussion

Practical projection of images though MMF has been a challenging task requiring non trivial interferometric methods to measure the complex field at the output of the fiber in the transmission method approach. The system response $H(\cdot)$ (the system here being the forward path from the SLM to the camera) is then the transmission matrix itself. Therefore, the SLM patterns corresponding to the desired target outputs are achieved by inverting $H(\cdot)$ using one of many algorithms proposed in the literature.

Alternatively, in our proposed approach, the two sub-networks G and D estimate the response function of the system $H(\cdot)$ from multiple input-output examples where outputs are only partially measured (phase is lost with the intensity-only detection). In analogy with the transmission matrix approach, G is basically $H^{-1}(\cdot)$ and D is $H(\cdot)$. Therefore, no additional step for inverting $H(\cdot)$ is required. This could be another advantage of the neural network method over its matrix counterpart. Because, as the size of $H(\cdot)$ increases with the 4th power of the fiber core size, inverting $H(\cdot)$ becomes non trivial and challenging.

Markedly, the necessity of using two sub-networks together for generating SLM patterns of the target camera images is even critical. This can be better understood when the two sub-networks are replaced entirely with one single network that is trained to retrieve the SLM images from the amplitude-only camera images. This new network is then trained with pairs of speckle images obtained on the camera as the input of the network and the SLM images as the output. Once trained, it is then fed with a desired target image to predict an SLM image thereof. As outlined with details in the Supplementary materials, the predicted SLM images obtained in this way produce projected images with significantly lower fidelities. The superiority of the two sub-network approach over the single network approach is very much indebted to sub-network D learning the forward path of the optical propagation inside the fiber. This allows the sub-network G to immediately evaluate the projection performance of the SLM image it has produced and to adapt its parameters to obtain a better projection *in the course of training* whereas, in the single network approach, direct evaluation of the projection performance for the *target images* is not carried out. The latter is due to the fact that the network in the this approach has been

trained to be given speckle-like images which are completely different from the class of perceivable images that are desired to be projected. In other words, in this case, the network is expected to directly generalize to the class of the desired target images when only trained on speckle-like images, a task which is difficult for the network to fulfill.

The easy access to both the forward (D) and backward (G) propagation paths of light is not the only advantage of the neural network approach over the conventional transmission matrix method as the latter one also entails constant tracking of the phase to compensate the drift which further complicates its implementation. However, the neural network approach inherently learns to correct for the perturbations in the system. This can be inferred from the decorrelation plot in Supplementary Fig. X which shows the rate of the decrease in the correlation of a fixed reference pattern versus time (known as decorrelation). It can be observed that despite the presence of significant decorrelation, the neural network learns to correct for the drift as well. This could also be promising for applications in which the fiber configuration changes; such is the case in fiber-based endoscopic imaging.

Therefore, the simplicity of the optical setup in the fiber projector based on the neural networks is promising that it could be easily adapted to a wide range of applications: for example by using a scattering wall to project images to a viewer for 3D displays or for near the eye applications (augmented reality).

4. Materials and Methods

Experimental set-up: The experimental setup for image transmission through the fiber is depicted in Fig. 7. A continuous input beam at wavelength 780 nm is delivered to the system by the laser source (Mira Coherent 900). The beam entering the system (attenuated to an average power of 22 mW), is expanded and collimated by objective OBJ 1 (50x, numerical aperture (NA) = 0.65) lens L1 ($f=100$ mm) and then directed to the SLM. The beam spatially modulated by the phase-only SLM (HOLOEYE PLUTO) is imaged on the input facet of a multimode fiber using a 4-f system composed of L2 ($f=200$ mm) and OBJ 2 (60x, NA=0.85). After transmission through the graded-index fiber with length $L=30$ cm, core diameter $D=62.5$ mm and a NA of 0.275 (1200 number of fiber modes for one polarization), the output field is imaged onto the camera using an identical 4-f configuration.

Neural network architecture: The projector network, schematically shown in Fig. 2, is composed of two sub-networks: the Generator (G) and the Discriminator (D) which together generate the SLM patterns required to obtain the desired images at the output of the fiber. As depicted in Fig. 8, both of the two sub-networks have the architecture of a fully-connected neural network in which, the input images are feed to the network via the input layer and passed on to the output layer via weights $w_{i,j}$ connecting node i to node j . All the incoming connections at node n_j in the output-layer are first summed up and bias corrected via bias b_j and then passed on to the nonlinear unit with the nonlinearity function $\sigma(x) = 1/(1 + \exp(-x))$ known as Sigmoid. Thereby, the j -th output of the fully-connected layer reads as:

$$n_j = \sigma \left[\sum_i w_{i,j} n_i + b_j \right] \quad (1)$$

The training of the two networks is carried out in an alternating fashion. Figure 2b schematically illustrates the training procedure comprised of 3 sub-steps A-C:

A- first the training examples composed of the patterns on the SLM, denoted by X , and their corresponding amplitude patterns captured on the camera referred to as Y are collected.

B- the Discriminator is trained on examples obtained from sub-step A to emulate the physical forward path from the SLM to the camera. Accordingly, the discriminator is trained by minimizing the mean squared error between $\hat{Y} = D(X)$ and the ground truth labels Y , i.e.

$$MSE(\theta) = \frac{1}{N \times M \times M} \sum_{l=1}^N \sum_{i=1}^M \sum_{j=1}^M |\hat{Y}_{i,j}^l(\theta_D) - Y_{i,j}^l|^2 \quad (2)$$

where θ_D are weights and biases of the D, i and j are the indices of the neural network reconstructed image \hat{Y}^l and the label image Y^l belonging to the l -th image pairs, where l and N are the samples' mini-batch index and size, respectively, and M is the width and height of the images.

C- next is the training of the Generator. The inputs to the Generator, denoted by Z , are examples of the images that we wish to see on the camera. The output of the Generator, $G(Z)$, is passed through the Discriminator. The Discriminator's output, $D(G(Z))$, is then compared against the inputs of the Generator (i.e. Z) using the logarithm of the Pearson coefficient factor, i.e.

$$\log[(1 + \text{Pearson}(D(G(Z)), Z)) / 2] \quad (3)$$

where the Pearson coefficient factor is between variables x and y is defined as:

$$\text{Pearson}(x, y) = \frac{\sigma_{x,y}}{\sigma_x \sigma_y} \quad (4)$$

in which $\sigma_{x,y}$ is the covariance between x and y , σ_x and σ_y are the standard deviations of x and y , respectively.

Even though the back propagated error from this comparison reaches the Generator via propagation through the Discriminator, but the weights and biases of the Discriminator are kept constant while training the Generator.

Once the training step is complete, the target image is fed to G to produce the required SLM pattern that generates the desired image on the camera. This step is shown in the validation part in Fig. 2b. The training process can be repeated for several iterations to improve the fidelity between the target images and the projected images on the camera. Figure 9 plots the fidelity (2D correlation) trajectory of the projected image of letter "C" on the camera as well as the virtually projected image of letter "C"

via the neural network. It is clear that the required SLM image is retrieved rapidly after a few iterations.

It is interesting to note that a byproduct of the proposed scheme is learning the forward propagation path of light by the sub-network D. This is better understood from Fig. 9 in which the SLM image generated by sub-network G is subsequently sent through D to obtain the virtually projected images of letter “C”. Notably, the improvement in the quality of the virtually projected images is closely followed by an improvement of the experimental projected images on the camera. This further illustrates that the sub-network D is able to successfully emulate the forward propagation path of light with a high degree.

Neural network training technical details: Parameter update of the two networks is carried out using adaptive moment estimation optimization (ADAM) algorithm with a learning rate of 10^{-4} and mini-batch size of 32 on a NVIDIA GTX 1080 Titan GPU.

References

- 1 Spitz, E. & Werts, A. Transmission des images à travers une fibre optique. *Comptes Rendus Hebd. Des. Seances De. L Acad. Des. Sci. Ser. B* **264**, 1015 (1967)
- 2 Gover, A., Lee, C. P. & Yariv, A. Direct transmission of pictorial information in multimode optical fibers. *JOSA* **66**, 306–311 (1976).
- 3 Friesem, A. A., Levy, U. & Silberberg, Y. Parallel transmission of images through single optical fibers. *Proceedings of the IEEE* **71**, 208–221 (1983).
- 4 Yariv, A., AuYeung, J., Fekete, D. & Pepper, D. M. Image phase compensation and real-time holography by four-wave mixing in optical fibers. *Applied Physics Letters* **32**, 635–637 (1978).
- 5 Garibyan, O. V. *et al.* Optical phase conjugation by microwatt power of reference waves via liquid crystal light valve. *Optics Communications* **38**, 67–70 (1981).
- 6 Yamaguchi, I. & Zhang, T. Phase-shifting digital holography. *Optics letters* **22**, 1268–1270 (1997).
- 7 Cucho, E., Bevilacqua, F. & Depeursinge, C. Digital holography for quantitative phase-contrast imaging. *Optics letters* **24**, 291–293 (1999).
- 8 Papadopoulos, I. N., Farahi, S., Moser, C. & Psaltis, D. Focusing and scanning light through a multimode optical fiber using digital phase conjugation. *Optics express* **20**, 10583–10590 (2012).
- 9 Papadopoulos, I. N., Farahi, S., Moser, C. & Psaltis, D. High-resolution, lensless endoscope based on digital scanning through a multimode optical fiber. *Biomed. Opt. Express* **4**, 260–270 (2013).
- 10 Di Leonardo, R. & Bianchi, S. Hologram transmission through multi-mode optical fibers. *Optics express* **19**, 247–254 (2011).

- 10 Čižmár, T. & Dholakia, K. Shaping the light transmission through a multimode optical fibre: complex transformation analysis and applications in biophotonics. *Optics Express* **19**, 18871–18884 (2011).
- 11 Čižmár, T. & Dholakia, K. Exploiting multimode waveguides for pure fibre-based imaging. *Nature communications* **3**, 1027 (2012).
- 12 Bianchi, S. & Di Leonardo, R. A multi-mode fiber probe for holographic micromanipulation and microscopy. *Lab on a Chip* **12**, 635–639 (2012).
- 13 Andresen, E. R., Bouwmans, G., Monneret, S. & Rigneault, H. Toward endoscopes with no distal optics: video-rate scanning microscopy through a fiber bundle. *Optics letters* **38**, 609–611 (2013).
- 14 Choi, Y. *et al.* Scanner-free and wide-field endoscopic imaging by using a single multimode optical fiber. *Physical review letters* **109**, 203901 (2012).
- 15 Caravaca-Aguirre, A. M., Niv, E., Conkey, D. B. & Piestun, R. Real-time resilient focusing through a bending multimode fiber. *Optics express* **21**, 12881–12887 (2013).
- 16 Gu, R. Y., Mahalati, R. N. & Kahn, J. M. Design of flexible multi-mode fiber endoscope. *Optics express* **23**, 26905–26918 (2015).
- 17 Loterie, D. *et al.* Digital confocal microscopy through a multimode fiber. *Optics express* **23**, 23845–23858 (2015).
- 18 Popoff, S., Lerosey, G., Fink, M., Boccarda, A. C. & Gigan, S. Image transmission through an opaque material. *Nat. Commun.* **1**, 81 (2010).
- 19 LeCun, Y., Bengio, Y. & Hinton, G. Deep learning. *Nature* **521**, 436–444 (2015).
- 20 McCann, M. T., Jin, K. H. & Unser, M. Convolutional neural networks for inverse problems in imaging: A review. *IEEE Signal Process Mag.* **34**, 85–95 (2017).
- 21 Rivenson, Y. *et al.* Deep learning microscopy. *Optica* **4**, 1437–1443 (2017).
- 22 Molesky, S. *et al.* Inverse design in nanophotonics. *Nature Photonics* **12**, 659 (2018).
- 23 Paruzzo, F. M. *et al.* Chemical shifts in molecular solids by machine learning. *Nature communications* **9**, 4501 (2018).
- 24 Rahmani, B., Loterie, D., Konstantinou, G., Psaltis, D. & Moser, C. Multimode optical fiber transmission with a deep learning network. *Light: Science & Applications* **7**, 69 (2018).
- 25 Borhani, N., Kakkava, E., Moser, C. & Psaltis, D. Learning to see through multimode fibers. *Optica* **5**, 960–966 (2018).
- 26 Caramazza, P., Moran, O., Murray-Smith, R. & Faccio, D. Transmission of natural scene images through a multimode fibre. *Nature communications* **10**, 2029 (2019).
- 27 Li, Y., Xue, Y. & Tian, L. Deep speckle correlation: a deep learning approach toward scalable imaging through scattering media. *Optica* **5**, 1181–1190 (2018).
- 28 Li, S., Deng, M., Lee, J., Sinha, A. & Barbastathis, G. Imaging through glass diffusers using densely connected convolutional networks. *Optica* **5**, 803–813 (2018).
- 29 Turpin, A., Vishniakou, I. & Seelig, J. Light scattering control in transmission and reflection with neural networks. *Optics express* **26**, 30911–30929 (2018).

30 Psaltis, D., Sideris, A. & Yamamura, A. A. A multilayered neural network controller. *IEEE control systems magazine* **8**, 17–21 (1988).

31 Cohen G, Afshar S, Tapson J, van Schaik A. EMNIST: An extension of MNIST to handwritten letters. arXiv preprint arXiv:1702.05373, (2017).

32 Davis, J. A., Cottrell, D. M., Campos, J., Yzuel, M. J. & Moreno, I. Encoding amplitude information onto phase-only filters. *Applied optics* **38**, 5004–5013 (1999).

Figures

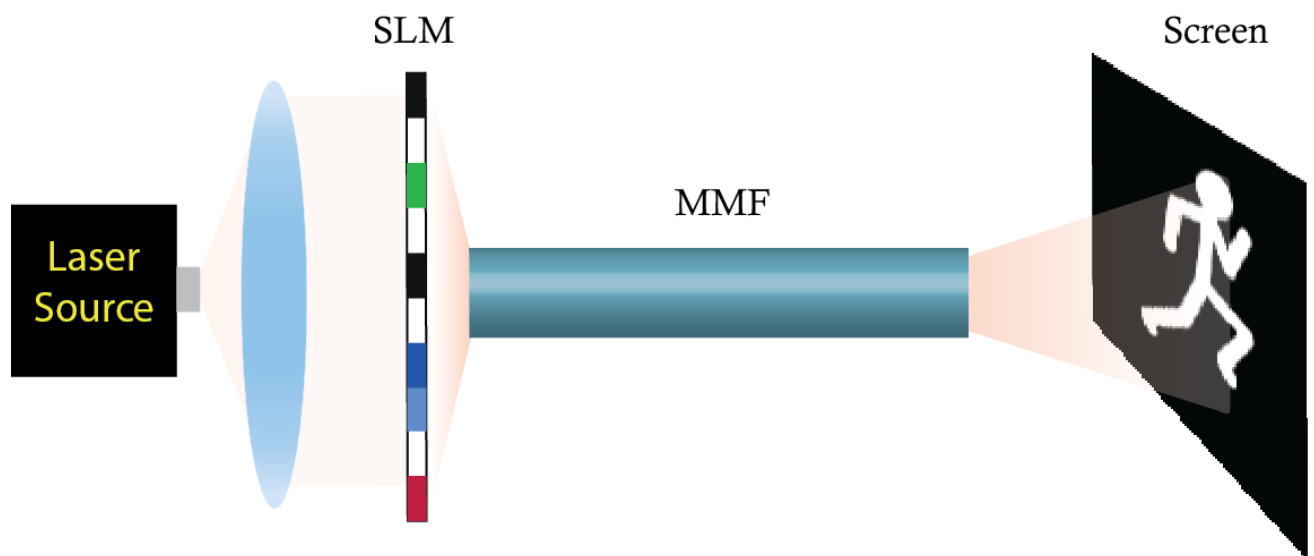


Figure 1. Fiber projector: The schematic of the multimode optical fiber projector is shown. The setup consists of a laser source, a light modulator (SLM), a MMF, and a screen. Wavefront shaping is required to undo the scrambling of the MMF. This wavefront shaping is carried out by a neural network. The network is given the desired image that is to be projected on the screen and the appropriate wavefront is readily given by the network.

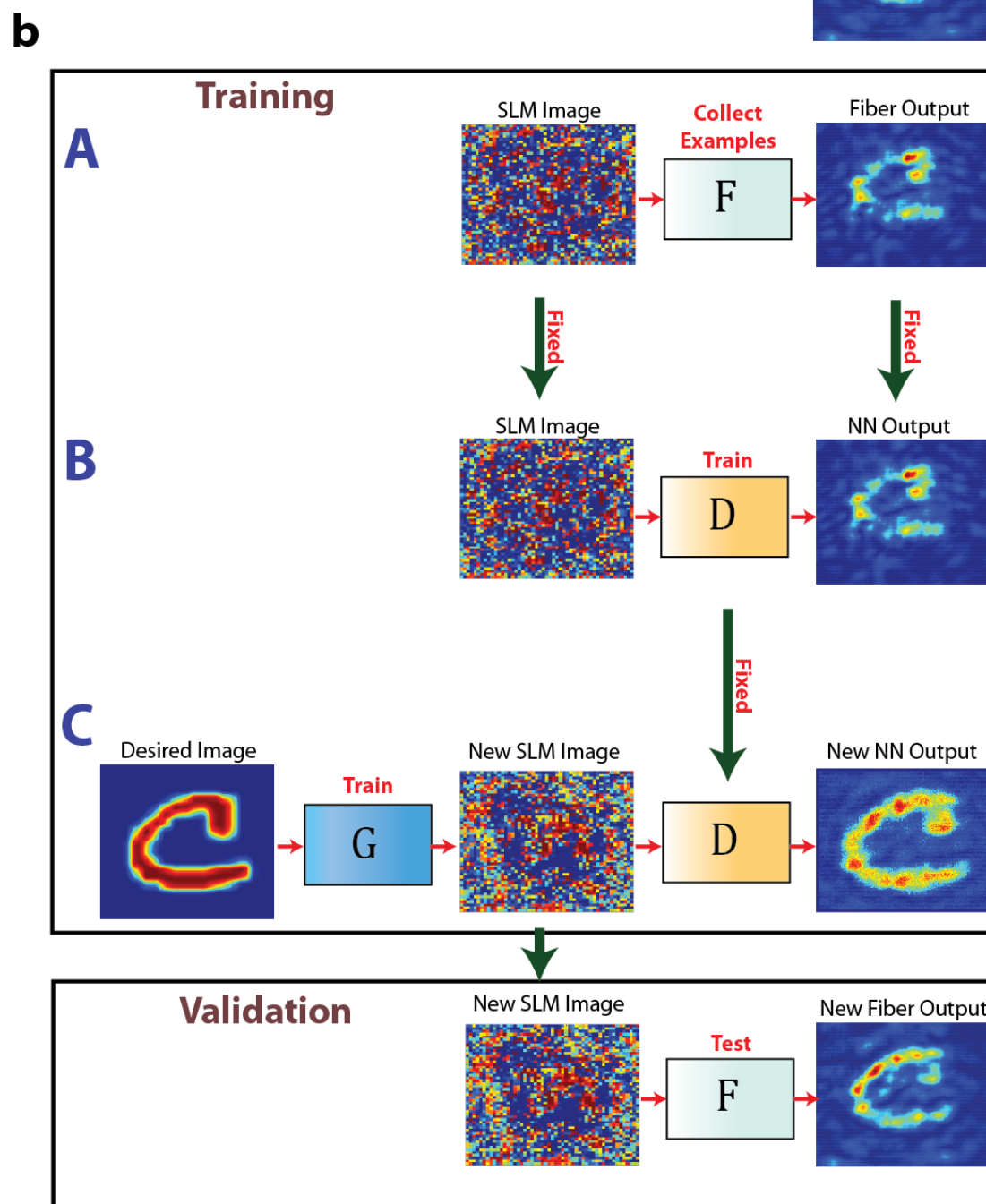
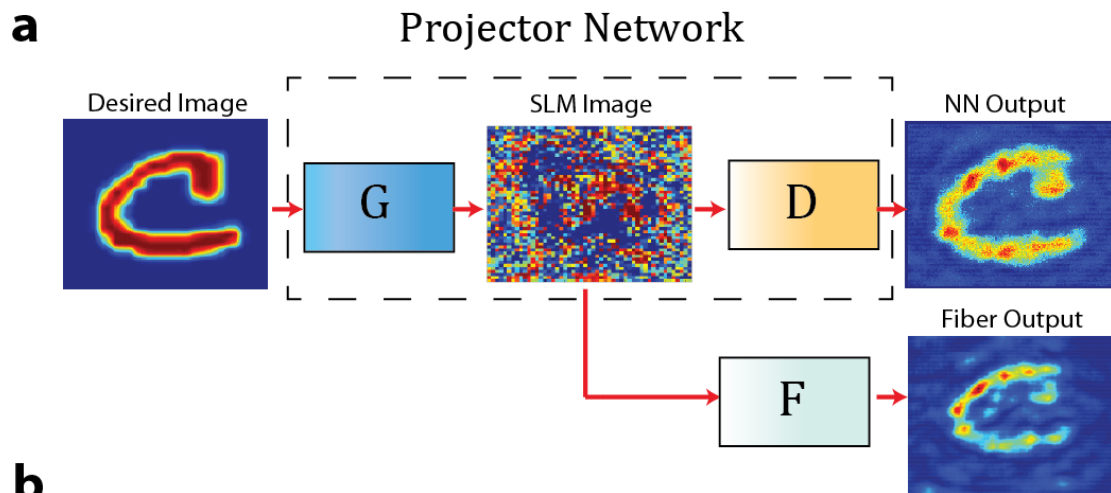


Figure 2. Neural network's architecture, training and validation procedure: (a) the overall schematic of the projector network comprises two sub-networks: a discriminator (D) and a generator (G) are shown. Once trained, the sub-network G accepts the target pattern desired to be projected at the output of the MMF and accordingly generates an SLM image corresponding to that pattern. The role of the sub-network D, which is trained to emulate the optical forward path SLM-MMF-camera, is to help the network G in the training step to come up with SLM patterns which result in projected images on the camera with higher fidelities. In this diagram, the fiber, the discriminator and generator sub-networks are denoted by F, D and G, respectively. The training procedure is carried out in three steps: A- a number of experimental examples from the SLM images to the amplitude-only images on the camera are obtained. B- the sub-network D is trained on these image to learn to map the SLM images to camera images; hence D is essentially learning the optical forward path SLM-MMF-camera. In the step C-, the network weights of D are fixed and sub-network G is trained with target images as input and producing an SLM image corresponding to the target image. The SLM image is then passed to the fixed sub-network D which produces an estimate of the fiber output based on the SLM image it received. The error between the output of D and the target image (input of G) is back propagated to G to updates its trainable weights and biases. The validation procedure is carried out by feeding the target image to the trained sub-network G and acquiring the appropriate SLM image corresponding to that target image.

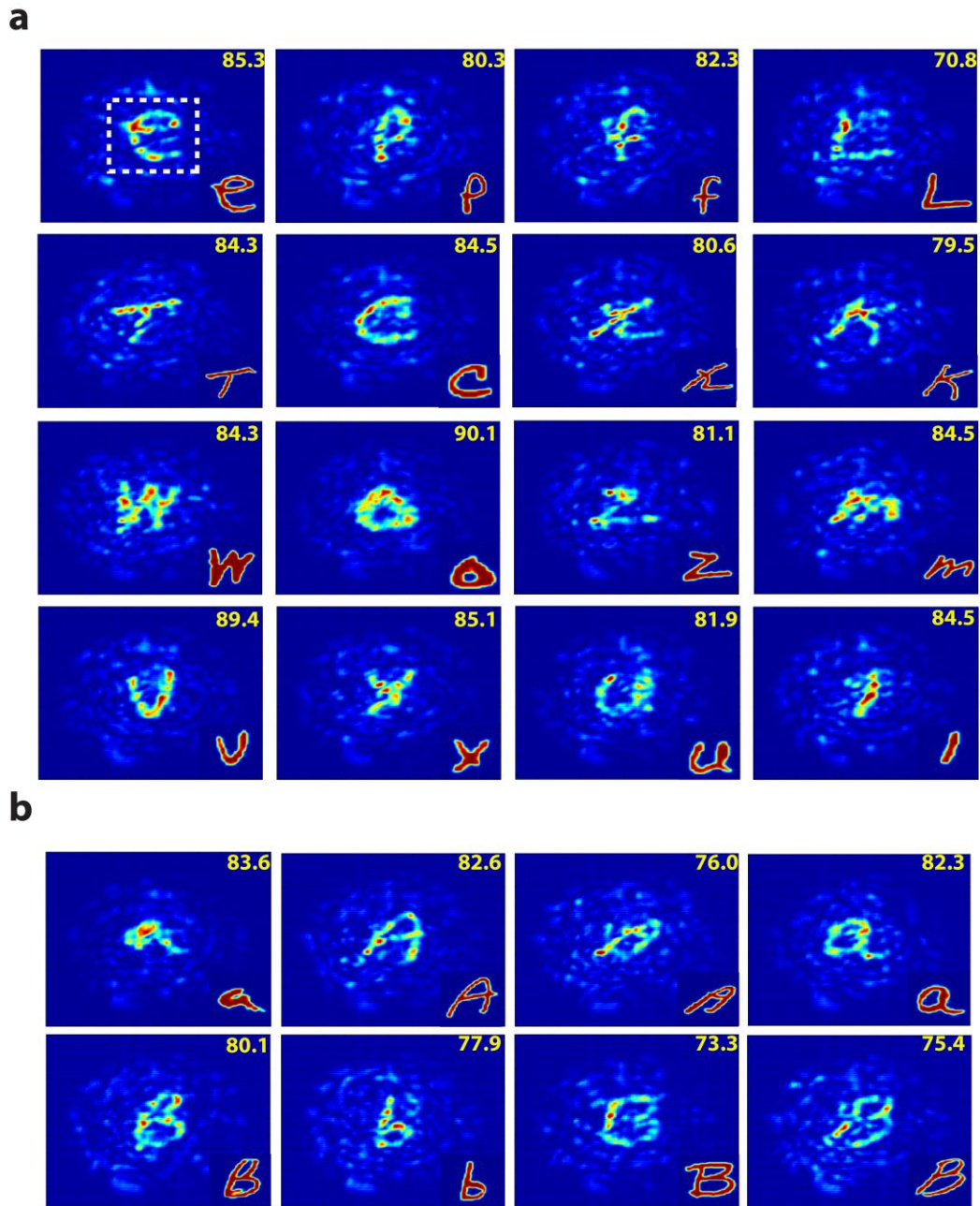


Figure 3. Latin alphabet training and test set image projection: Examples of the projected images from the Latin alphabet (a) train and (b) test dataset captured on the camera are shown. The target image, shown on the bottom right corner of each image, is fed to the neural network to generate the appropriate SLM pattern that produces that desired target image on a rectangular area of size 200×200 pixels ($1.6 \times 1.6 \text{ mm}^2$) corresponding to the central part of the fiber's facet FOV. This area is shown as a dashed box on the top left image. The fidelity of the projected image with respect to its corresponding grayscale target image is shown as inset.

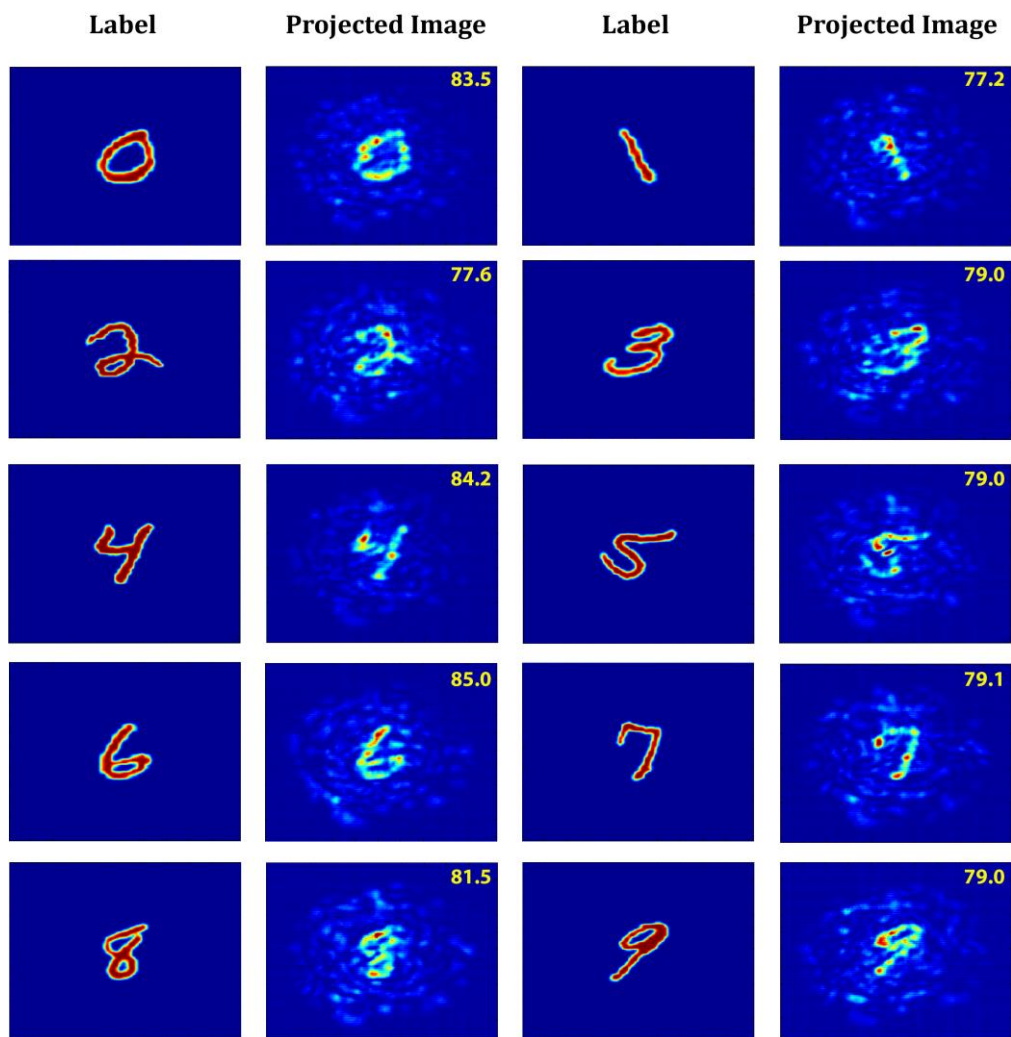


Figure 4. Neural network generalization of image projection to handwritten digits set: Examples of the projected images from the MNIST handwritten digits dataset are provided. Target images, shown next to the projected images, are blindly fed to the neural network which was trained only on alphabet characters. The neural network generated SLM patterns are sent through the fiber and the outputs of the fiber are captured on the camera. The fidelity of the projected image with respect to its corresponding grayscale target image is shown as inset.

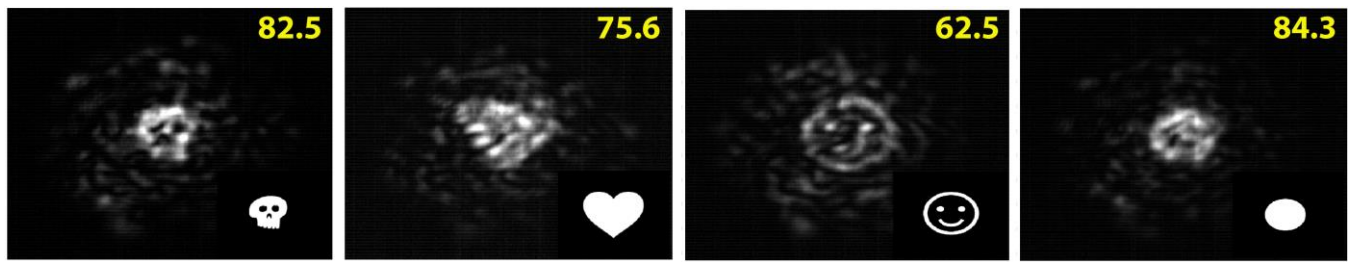


Figure 5. Neural network generalization of image projection to random drawings: Examples of the projected random drawings (a skull a heart, a smiley, a circle) are provided. Target images, shown in bottom right corner, are blindly fed to the neural network which was trained only on alphabet characters. The neural network generated SLM patterns are sent through the fiber and the outputs of the fiber are captured on the camera. The fidelity of the projected image with respect to its corresponding grayscale target image is shown as inset.



Figure 6. Running person image projection through the fiber: The neural network trained on Latin alphabet characters is used to generate the required SLM pattern that produces a drawing of a running man in an area of 200×200 pixels ($1.6 \times 1.6 \text{ mm}^2$) corresponding to the central part of the fiber's facet FOV. The desired target image (left), the corresponding SLM image (middle) and the projected image (right) are depicted. The fidelity of the projected image with respect to its desired image is shown as inset. An animation of the target image is provided in the Supplementary Materials I.

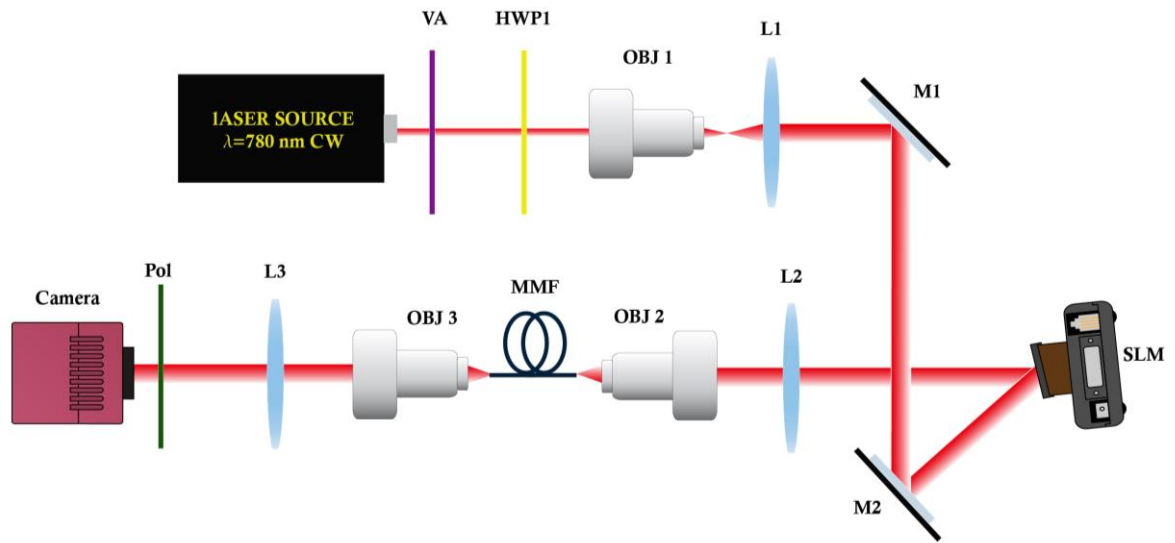


Figure 7. Optical setup: Detailed diagram of the optical setup. VA: variable attenuator; HWP1: half-wave plate; L1: $f = 100\text{mm}$ lens; L2: $f = 200\text{mm}$ lens; L3: $f = 200\text{mm}$ lens; OBJ1: infinity corrected 50x microscope objective lens; OBJ2, OBJ3: 60x microscope objective; Pol: linear polarizer; SLM: spatial light modulator; M1, M2: mirror; MMF: multimode fiber.

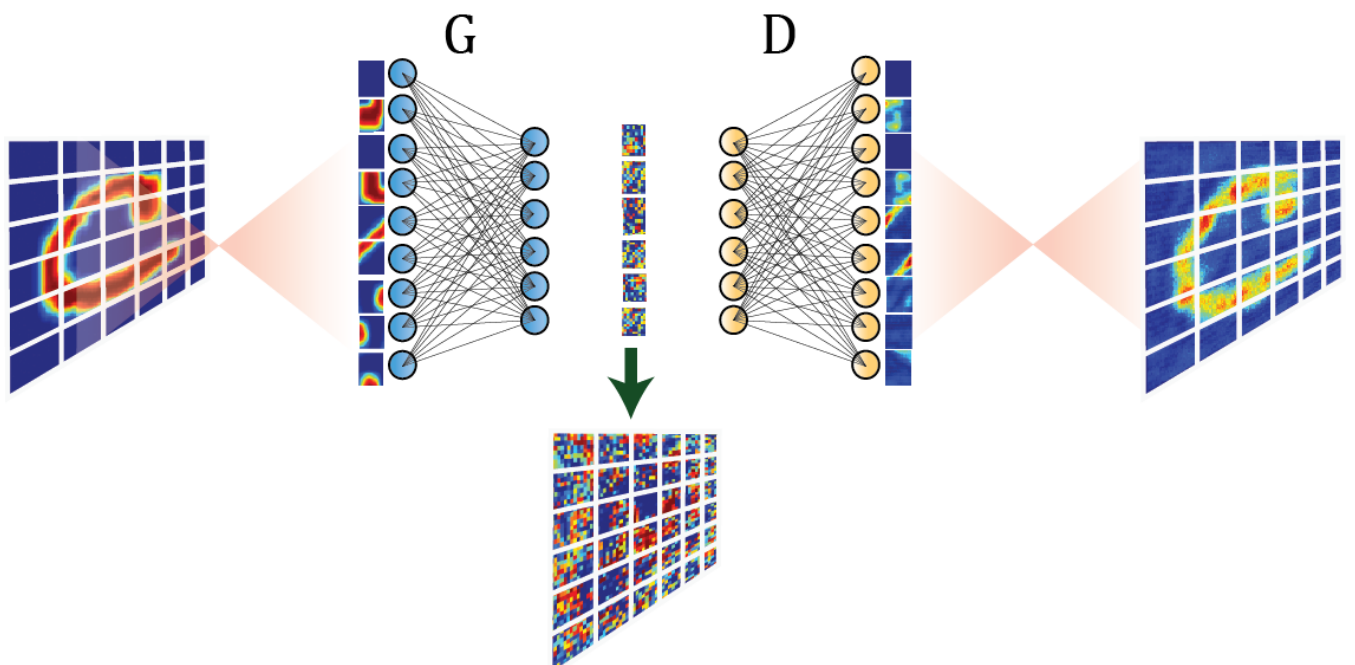


Figure 8. Neural network's architecture. Both of the two sub-networks have the architecture of a fully-connected network. Thereby, the input images to the network G is first flattened out (from size 200×200 pixels to 40000×1 vectors) and then fed to the network. In the training step, the output vectors (size 2601×1) are passed on to the second sub-network D that produces the virtual neural network output images

of the target images (size 200×200). Once trained, the output vectors of the sub-network G can be directly reshaped to produce SLM images (from size 2601×1 to 51×51 pixels). If these SLM images are sent through the fiber, they produce projected images on the camera that are similar to the target images. Refer to Fig. 7 for a detailed explanation on the training procedure of the two sub-networks.

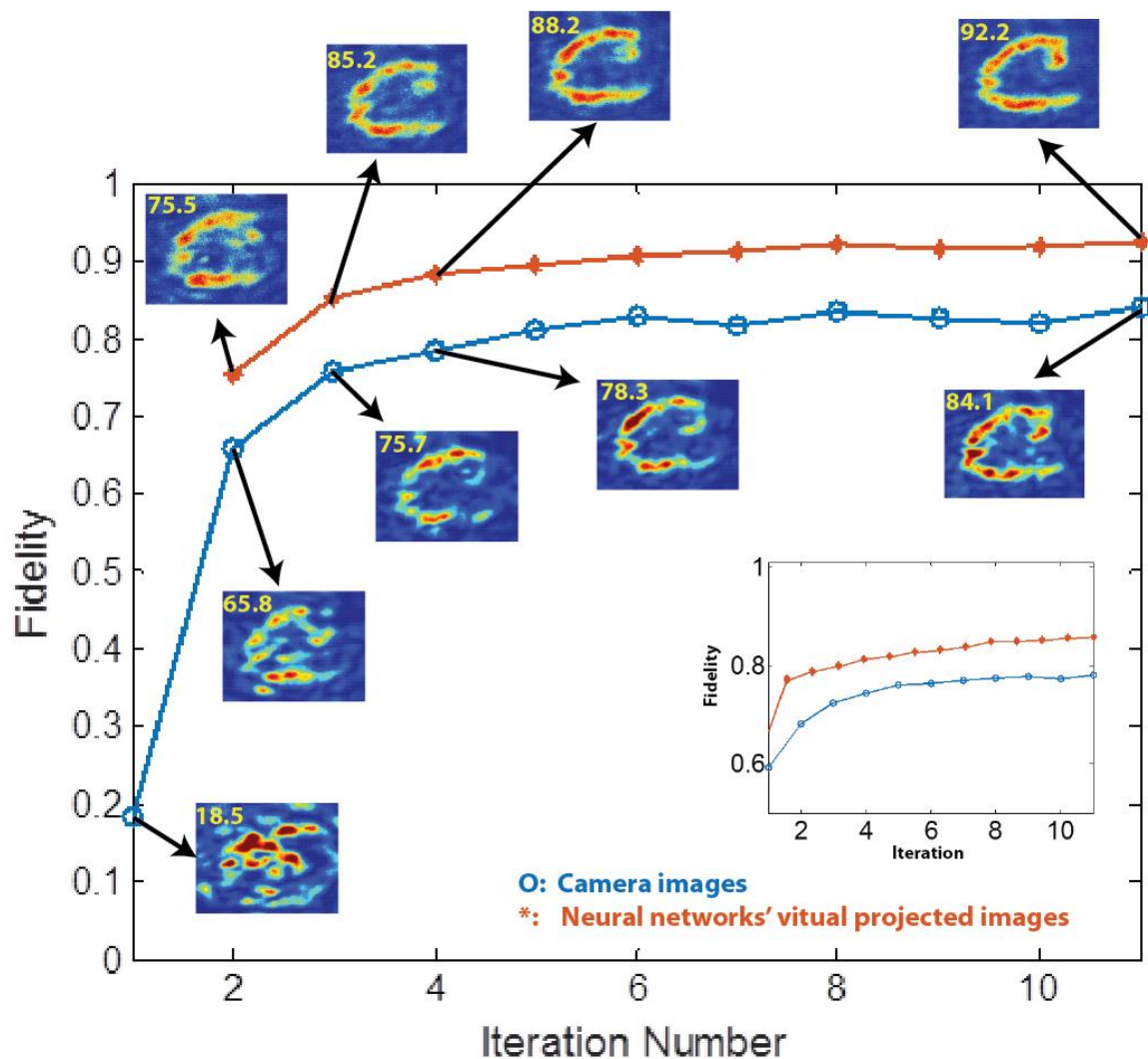


Figure 9. Training trajectory of the projector network. The fidelity trajectory of letter C's projected image on the camera (blue solid line) as well as the fidelity of the virtually projected image through the sub-network D (red solid line) while training the neural network. The projected images at various intermediate iterations are also shown. The fidelity reaches 80% after three iterations. Average fidelity trajectory of the entire 20000 Latin alphabet dataset is also plotted as inset.